PHYSOR 2014 – The Role of Reactor Physics Toward a Sustainable Future
The Westin Miyako, Kyoto, Japan, September 28 – October 3, 2014, on CD-ROM (2014)

EXTENSION OF LINEAR SOURCE MOC METHODOLOGY TO ANISOTROPIC SCATTERING IN CASMO5

Rodolfo Ferrer, Joel Rhodes*
Studsvik Scandpower, Inc.
1070 Riverwalk Drive, Suite 150, Idaho Falls ID 83402, USA
rodolfo.ferrer@studsvik.com
joel.rhodes@studsvik.com

ABSTRACT

The Linear Source (LS) spatial approximation, previously implemented in the Method of Characteristic (MOC) transport solver under the assumption of isotropic scattering, is extended to account for anisotropic scattering. The generalized formulation results in the representation of the angular moments of the flux as a linearly varying function within each source region and is fully compatible with Coarse-Mesh Finite Difference (CMFD) acceleration. The main set of equations for this anisotropic-source LS MOC method are derived in this work and numerical results are presented for critical assembly test cases. The results show improvement in the accuracy of the transport solution, but also an increase in run time and storage relative to the LS isotropic scattering implementation.

Key Words: **Anisotropic, Scattering, Linear Source, MOC, Transport, CASMO.**

1. INTRODUCTION

The current two-dimensional transport solver used in Studsvik Scandpower's CASMO5 lattice physics code is based on the Linear Source (LS) spatial approximation [1]. The LS approximation is a generalization of the "flat source" assumption, typically used in conjunction with isotropic scattering in the Method of Characteristics (MOC) solution scheme [2], [3]. In combination with Coarse-Mesh Finite Difference (CMFD) acceleration [4], the LS MOC is an accurate and efficient approach for the solution of two-dimensional transport problems, and hence, the generation of accurate assembly-averaged nodal data for downstream LWR reactor analysis [5].

In order to utilize the computational efficiency of the isotropic scattering assumption, a transport correction is typically applied to the total macroscopic cross-section to maintain accuracy and account for the anisotropy of the scattering source [6]. While the transport correction works well for single assembly calculations with reflective boundary conditions, an explicit representation of the anisotropic scattering source is needed to accurately solve a wider range of problems, such as multi-assembly models of critical assemblies involving a high degree leakage. The validation of the transport correction is often performed by determining whether the accuracy of the transport-corrected isotropic source solution is adequate with respect to the high-order, anisotropic source transport solution.

The ability to perform two-dimensional transport calculations with anisotropic scattering, under the assumption of spatially 'flat' source regions, has been present in CASMO for some time [7]. The recent implementation of the LS approximation prompted the extension of the LS MOC formulation to account for anisotropic scattering. Previous developments in the area of spatially

* http://www.studsvik.com/nfa

linear source approximations, in conjunction with anisotropic scattering, include the current-based linearly-anisotropic scheme [8] and the nonlinear linear surface method [9]. An algebraically linear, high-order moment based MOC was previously derived, but only the isotropic source approximation implemented and numerically tested [10]. In the next section the set of equations for the anisotropic-source LS scheme are derived starting from the transport equation under the assumption of anisotropic scattering along a characteristic direction.

2. THEORY

The differential form of the transport equation along a distance s_m in the azimuthal direction a and polar direction p, denoted by the double index $m = (a, p)$, of a track k within source region i is given by

$$\frac{d\psi^g_{m,k,i}}{ds_m} + \Sigma^g_{T,i}\psi^g_{m,k,i} = q^g_{m,k,i}(s_m) \tag{1}$$

where $\psi^g_{m,k,i}$, $q^g_{m,k,i}$ and $\Sigma^g_{T,i}$ correspond to the angular flux, total source, and total cross-section for energy group g, respectively. The total source along the track distance in Eq. (1) is given by the following expression

$$q^g_{m,k,i}(s_m) = \bar{q}^g_{m,k,i} + \hat{q}^g_{m,i}\left(s_m - s^c_{m,k,i}\right) \tag{2}$$

Note that in Eq. (2) the track length is given by $s_{m,k,i}$, such that $0 \le s_m \le s_{m,k,i}$ and $s_{m,k,i} = \tau_{a,k,i}/\sin\theta_p$, where $\tau_{a,k,i}$ is the track length in the azimuthal direction after being re-normalized to preserve the source region volume. In addition, $s^c_{m,k,i} = s_{m,k,i}/2$ and the expansion coefficients $\bar{q}^g_{m,k,i}$ and $\hat{q}^g_{m,i}$ are defined later. The integration of Eq. (1) along the track distance, given the linear source in Eq. (2), results in the following expression

$$\psi^g_{m,k,i}(s_m) = \psi^g_{m,k,i}(0) + \left(\frac{\bar{q}^g_{m,k,i}}{\Sigma^g_{T,i}} - \psi^g_{m,k,i}(0)\right)E_1\left(\varepsilon^g_{m,i}\right) + \frac{\hat{q}^g_{m,i}}{2\left(\Sigma^g_{T,i}\right)^2}E_3\left(\varepsilon^g_{m,i}\right) \tag{3}$$

where $\varepsilon^g_{m,i} = \Sigma^g_{T,i}s_m$ is the optical thickness and $\psi^g_{m,k,i}(0)$ denotes the incoming angular flux. The efficient numerical evaluation of the expressions denoted as $E_1\left(\varepsilon^g_{m,i}\right)$ and $E_3\left(\varepsilon^g_{m,i}\right)$ in Eq. (3), even in the case of optically thin medium, is detailed in a previous work [1]. These expressions correspond to the integration of the exponential function along with track length. The outgoing angular flux is obtained by evaluating Eq. (3) at the track end point, i.e. $s_m = s_{m,k,i}$. The average and first-order spatial moment of the angular flux along a given track distance are defined as follows, respectively

$$\bar{\psi}^g_{m,k,i} = \frac{1}{s_{m,k,i}}\int_0^{s_{m,k,i}} \psi^g_{m,k,i}(s_m)ds_m \tag{4}$$

$$\hat{\psi}^g_{m,k,i} = \frac{1}{s_{m,k,i}}\int_0^{s_{m,k,i}} s_m\psi^g_{m,k,i}(s_m)ds_m \tag{5}$$

The balance equation along each track length is obtained by integrating Eq. (1) over the track length

$$\frac{\psi^g_{m,k,i}(s_{m,k,i}) - \psi^g_{m,k,i}(0)}{s_{m,k,i}} + \Sigma^g_{T,i}\bar{\psi}^g_{m,k,i} = \bar{q}^g_{m,k,i} \tag{6}$$

In an analogous fashion, the first-order spatial moment is obtained from Eq. (3) by taking the first-order spatial moment of the equation, which results in the following relation

$$\hat{\psi}^g_{m,k,i} = \psi^g_{m,k,i}(0)s^c_{m,k,i} + \left(\frac{\bar{q}^g_{m,k,i}}{\Sigma^g_{T,i}} - \psi^g_{m,k,i}(0)\right)\frac{\Gamma_1(\varepsilon^g_{m,i})}{\Sigma^g_{T,i}} + \frac{\hat{q}^g_{m,i}}{2(\Sigma^g_{T,i})^2}s_{m,k,i}\Gamma_3(\varepsilon^g_{m,i}) \tag{7}$$

The efficient numerical evaluation of $\Gamma_1(\varepsilon^g_{m,i})$ and $\Gamma_3(\varepsilon^g_{m,i})$ is detailed in previous work [1]. Given expansion coefficients of the source in Eq. (2) and an incoming angular flux, the outgoing angular flux can be obtained from Eq. (3), the average angular flux obtained from Eq. (6), and the first-order spatial moment obtained from Eq. (7). Since most problems of interest in numerical transport calculations require some sort of iteration on the source, the relationship between the angular fluxes and sources must be established.

In order to evaluate the source along the track length, defined by Eq. (2), the two-dimensional anisotropic scattering source is defined by the following equation

$$q^g_{m,i}(x,y) = \sum_{l=0}^{L}\sum_{r=-l}^{l} R_\alpha(\varphi_a,\mu_p)\sum_{g'}\Sigma^{g'\to g,l}_{s,i}\phi_i^{g',\alpha}(x,y) + F_i^g(x,y) \tag{8}$$

where L is the anisotropic scattering expansion order, $\mu_p = \cos\theta_p$, $\alpha = (l,r)$ is a double index, and $R_\alpha(\varphi_a,\mu_p)$ is the real spherical harmonics function. The real spherical harmonics function requires the evaluation of the associated Legendre polynomials, defined as

$$P_l^r(\mu_p) = (-1)^r(1-\mu_p^2)^{r/2}\frac{d^r}{d\mu_p^r}P_l(\mu_p), r \geq 0 \tag{9}$$

The real spherical harmonics function is defined as follows

$$R_\alpha(\varphi_a,\mu_p)=\begin{cases}\sqrt{\dfrac{2l+1}{4\pi}}\sqrt{2\dfrac{(l-r)!}{(l+r)!}}P_l^r(\mu_p)\cos(r\varphi_a), & r>0\\ \sqrt{\dfrac{2l+1}{4\pi}}P_l^0(\mu_p), & r=0\\ \sqrt{\dfrac{2l+1}{4\pi}}\sqrt{2\dfrac{(l-r)!}{(l+r)!}}P_l^r(\mu_p)\sin(r\varphi_a), & r<0\end{cases} \tag{10}$$

Hence, the moments-to-discrete operator is defined by Eq. (8), which requires the evaluation of Eqs. (9) and (10), for each angular direction. The space-dependent angular moments of the flux are defined as follows

$$\phi_i^{g,\alpha}(x,y)=\phi_i^{g,\alpha}+\phi_{i,x}^{g,\alpha}x+\phi_{i,y}^{g,\alpha}y \tag{11}$$

Note that the spatial dependence (x,y) in Eqs. (8) and (11) is defined with respect to a local coordinate system in each source region. The computation of the local coordinate system, centered about the trajectory-based centroid, is explained in more detail in a previous publication [1]. Substituting Eq. (11) into Eq. (8) results in an expression relating $\{\phi_i^{g,\alpha},\phi_{i,x}^{g,\alpha},\phi_{i,y}^{g,\alpha}\}$ and the source $q_{m,i}^g(x,y)$. However, in order to perform the 'transport sweep', the expansion coefficients of the following linear source must be determined

$$q_{m,i}^g(x,y)=q_{m,i}^g+q_{m,i,x}^g x+q_{m,i,y}^g y \tag{12}$$

Recalling the trajectory-based spatial moment operator from [1]

$$\frac{1}{V_i}\int f(\vec{r})g(\vec{r})dV=\frac{4\pi}{V_i}\sum_m \omega_m \sin\theta_p \sum_k \int_0^{s_{m,k,i}} f(s_m)g(s_m)ds_m\,\delta A_a \tag{13}$$

and taking the constant, x- and y-moments of Eq. (12) results in the following equations

$$M_{i,xx}q_{m,i,x}^g+M_{i,xy}q_{m,i,y}^g=Q_{m,i,x}^g \tag{14}$$

$$M_{i,xy}q_{m,i,x}^g+M_{i,yy}q_{m,i,y}^g=Q_{m,i,y}^g \tag{15}$$

where

$$M_{i,xx}=\frac{4\pi}{V_i}\sum_m \omega_m \sin\theta_p \sum_k \int_0^{s_{m,k,i}} [x(s_m)]^2 ds_m\,\delta A_a \tag{16}$$

$$M_{i,yy} = \frac{4\pi}{V_i} \sum_m \omega_m \sin\theta_p \sum_k \int_0^{s_{m,k,i}} [y(s_m)]^2 ds_m \, \delta A_a \tag{17}$$

$$M_{i,xy} = \frac{4\pi}{V_i} \sum_m \omega_m \sin\theta_p \sum_k \int_0^{s_{m,k,i}} x(s_m) y(s_m) ds_m \, \delta A_a \tag{18}$$

The local coordinate system is defined such that $M_{i,x} = 0$ and $M_{i,y} = 0$. Substituting Eq. (11) into Eq. (8) and taking the constant, x- and y-moments, defined by Eq. (13), results in explicit expressions for the right hand side of Eqs. (14), (15), i.e. $Q^g_{m,i,x}$ and $Q^g_{m,i,y}$. The region-averaged or constant expansion coefficient is equal to the region-averaged anisotropic source $q^g_{m,i}$ and is given by the following equation

$$q^g_{m,i} = \sum_{l=0}^{L} \sum_{r=-l}^{l} R_\alpha(\varphi_a, \mu_p) \sum_{g'} \Sigma^{g' \to g,l}_{s,i} \phi_i^{g',\alpha} + F_i^g(x,y) \tag{19}$$

Analogous expressions to Eq. (19) can be derived relating $Q^g_{m,i,x}$ and $Q^g_{m,i,y}$ to the spatial moments of the angular moments of the flux, $\Phi^{g,\alpha}_{i,x}$ and $\Phi^{g,\alpha}_{i,y}$. The values for $\phi_i^{g,\alpha}$, $\Phi^{g,\alpha}_{i,x}$ and $\Phi^{g,\alpha}_{i,y}$ are accumulated during the transport sweep. These expressions are obtained by taking the spatial moments of the angular discrete-to-moment operator. For example, the region-averaged angular moment of the flux is given by the following expression

$$\phi_i^{g,\alpha} = \frac{4\pi}{V_i} \sum_m \omega_m \delta A_a \sum_k R_\alpha(\varphi_a, \mu_p) \int_0^{s_{m,k,i}} \psi^g_{m,k,i}(s_m) ds_m \tag{20}$$

Substituting Eq. (4) into Eq. (20) and defining the angular flux $\psi^g_{m,i}$ integrated over all tracks k crossing region i in direction m

$$\bar{\Psi}^g_{m,i} = \sum_k \bar{\psi}^g_{m,k,i} s_{m,k,i} \tag{21}$$

results in the following expression for the average or constant spatial moment of the angular moment α

$$\phi_i^{g,\alpha} = \frac{4\pi}{V_i} \sum_m \omega_m \delta A_a R_\alpha(\varphi_a, \mu_p) \bar{\Psi}^g_{m,i} \tag{22}$$

Substituting Eq. (6) into Eq. (21) results in an explicit expression for the angular flux integrated over all tracks k. Analogous expressions can be derived relating the x- and y-moments of each angular flux moments, $\Phi^{g,\alpha}_{i,x}$ and $\Phi^{g,\alpha}_{i,y}$,

$$\Phi_{i,x}^{g,\alpha} = \frac{4\pi}{V_i}\sum_m \omega_m \delta A_a \sum_k R_\alpha(\varphi_a,\mu_p)\int_0^{s_{m,k,i}} x(s_m)\psi_{m,k,i}^g(s_m)ds_m \tag{23}$$

$$\Phi_{i,y}^{g,\alpha} = \frac{4\pi}{V_i}\sum_m \omega_m \delta A_a \sum_k R_\alpha(\varphi_a,\mu_p)\int_0^{s_{m,k,i}} y(s_m)\psi_{m,k,i}^g(s_m)ds_m \tag{24}$$

Given a fixed track length, the relation between the spatial coordinates as a function of track distance s_m is determined by the incoming or outgoing two-dimensional coordinates and the angular direction, e.g. $x(s_m) = \cos\varphi_a \sin\theta_p\, s_m/\xi_i + x_{m,k,i}^{in}$, where ξ_i is a normalization factor which preserves the source-region volume. Substituting these coordinates into Eqs. (23)-(24) provides the necessary expressions to evaluate the x- and y-moments of each angular flux moments, which require the computation of the first-order moment of the angular flux $\hat{\Psi}_{m,i}^g$ integrated over all tracks k crossing region i in direction m

$$\hat{\Psi}_{m,i}^g = \sum_k \hat{\psi}_{m,k,i}^g s_{m,k,i} \tag{25}$$

At the beginning of each angular sweep in direction m, the anisotropic source is evaluated given a set of angular flux moments for each spatial moment, using Eq. (19) and analogous expressions for $Q_{m,i,x}^g$ and $Q_{m,i,y}^g$. The source in angular direction m is determined by Eq. (2) and Eq. (12) by substituting explicit expression for $x(s_m)$ and $y(s_m)$, i.e.

$$\bar{q}_{m,k,i}^g = \frac{1}{4\pi}\left(q_{m,i}^g + q_{m,i,x}^g x_{a,k,i}^c + q_{m,i,y}^g y_{a,k,i}^c\right) \tag{26}$$

$$\hat{q}_{m,i}^g = \frac{1}{4\pi}\left(a_m^x q_{m,i,x}^g + a_m^y q_{m,i,y}^g\right)/\xi_i \tag{27}$$

where $x_{a,k,i}^c$ and $y_{a,k,i}^c$ are the track centroids, $a_m^x = \cos\varphi_a \sin\theta_p$, $a_m^y = \sin\varphi_a \sin\theta_p$. The source expansion coefficients allows for the computation of the region i average- and first-order spatial moment of the angular flux, defined by Eqs. (4) and (5), respectively. These track-length quantities are in turn accumulated for all angular directions and used to evaluate the angular moments, using the discrete-to-moment operators defined by Eqs. (22)-(24).

Once the transport sweep is finalized, the accumulated angular flux moments, the scalar flux and coarse-mesh net-currents are used to accelerate the scattering and fission iteration by applying CMFD acceleration. The coarse-mesh flux solution of the low-order transport-equivalent system is used to nonlinearly update the scalar flux and angular flux moments for all the spatial moments. Hence, no modifications are necessary to the CMFD acceleration.

2. NUMERICAL RESULTS

In order to verify the implementation, and compare the advantage of the LS MOC scheme relative to the flat source MOC, a set of benchmark cases were used to quantify the accuracy and efficiency of each method.

The B&W Series 3647 (Simple Criticals) experiments [11] consist of two very simple cores, (one circular and one square), as shown in Figure 1. These cores contain no heterogeneities (e.g., water holes, absorber holes, enrichment splits) and since the cores differ in size and shape, they present a wide range of radial leakage. Core I consists of 458 identical fuel pins (2.459 wt%) arranged in a circular shape, but has been symmetrized for our purposes. The axial leakage represents 2% of the total reactivity of the core. However, the radial leakage represent nearly 35%, hence this core is in a very high-leakage configuration. Core II consists of 1764 identical fuel pins (2.459 wt%) arranged in a square shape. The axial leakage represents 2% of the total reactivity of the core and the radial leakage represents roughly 15%, hence, this core is in a relatively low-leakage configuration. The two cores together – Core I and Core II – provide a very good indication of the accuracy with which radial leakage and anisotropic scattering can be modeled in CASMO5.

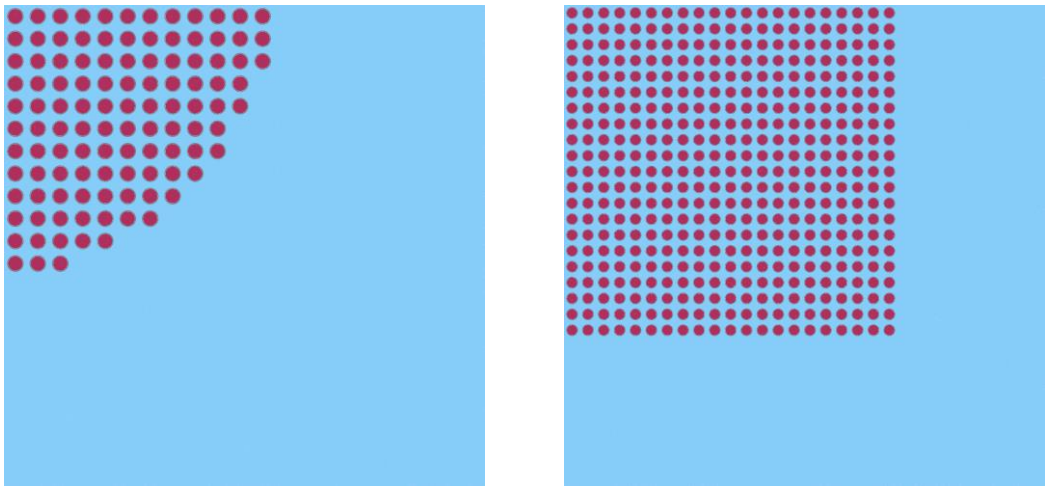

Figure 1. B&W Series 3647 (Simple Criticals) Core I and II on left and right, respectively.

The CASMO model for these cores is not as detailed as the criticality benchmark, since the purpose is to use a representative problem to test the LS solver. Three spatial grids, or meshes, were used in this study. The flat source and linear source cases use identical grids and the anisotropic source expansion order varied from 0 (isotropic) to 5. A third case, referred to as the reference case, uses a much finer mesh than the flat or linear source. The solver used for the reference case is the standard 'flat' source. In order to capture the anisotropic effects, a 95 energy-group structure was used to solve this problem. This is the default option in CASMO5 when modeling criticality benchmark problems. The angular discretization used for these problems consist of 64 azimuthal angles, 3 polar angles, and a 0.05 cm ray spacing. The same neutron data library was used for all three cases and it is based on the ENDF/B-VII.1 evaluation.

In the flat and linear source cases, the spatial mesh used for the pin cell regions involves 8 azimuthal source regions and four radial regions (fuel, gap, clad and coolant). The reflector region mesh is set to 1.0 cm^2 square cells. In the case of the reference model, the spatial mesh used for the pin cell region also involves 8 azimuthal source regions, but the radial regions are increased to 6, due to additional source regions in the coolant. These additional radial regions produce a finer coolant-region mesh. The reflector region mesh for the reference case is set to 0.1 cm^2 square cells. The spatial mesh parameter in the reference case are identical between the Core I and II. However, since the critical configurations are of different sizes, the total number of source regions differs between the two core models. The total number of source regions for the two cores is given in Table I.

Table 1. Total number of source regions in calculation.

B&W Simple Critical	**Flat/Linear**	**Reference**
Core I	2668	23255
Core II	6683	39487

The results for Core I & II, using the flat and linear source, are shown in Figure 2 and 3 below, respectively. A comparison between flat and linear source solver eigenvalue, relative to the eigenvalue from the reference case, is plotted as a function of the anisotropic source expansion order. The plotted quantity, labeled "delta$-k$", in pcm is defined as follows

$$\delta k = \left\| k - k_{ref} \right\| \times 10^5$$

where k is the eigenvalue from the flat or linear source case and k_{ref} is the eigenvalue from the reference case for the same anisotropic scattering order.

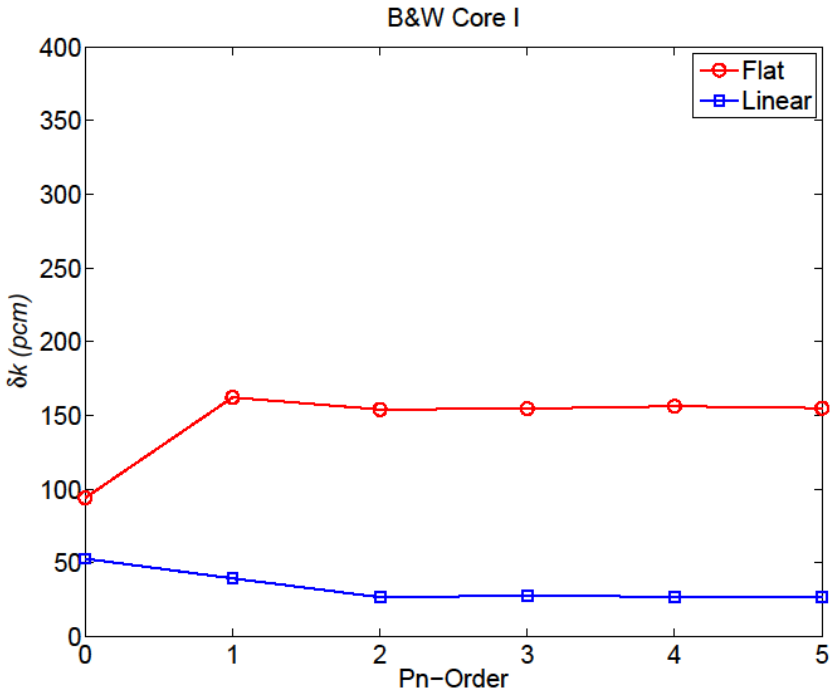

Figure 2. Eigenvalue comparison for Core I using flat and linear source.

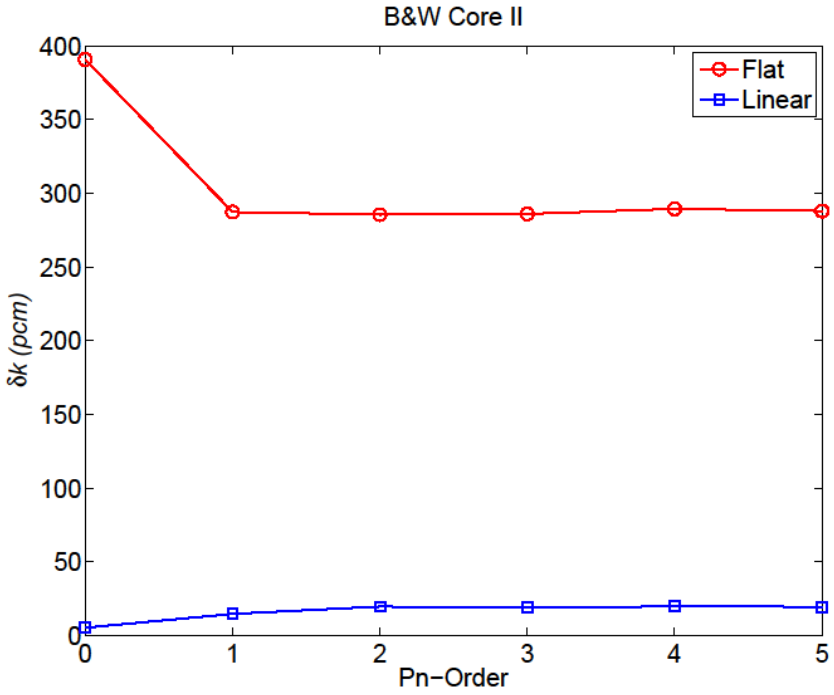

Figure 3. Eigenvalue comparison for Core II using flat and linear source.

Averaged over all scattering expansion order, the use of the linear source scheme improves the accuracy of the resulting eigenvalue, relative to the reference, by 113 pcm for Core I and 288 pcm for Core II, as compared to the flat source case. The difference between the linear source and reference case eigenvalues, which is well below 50 pcm, is caused by the fact that the computation of the condensation spectrum in CASMO is mesh-dependent, hence the reference case will use a slightly different spectrum to condense the 586-group neutron cross-section to the 95-group structure [7]. In addition, the degree of mesh refinement available in the code is not arbitrary.

Note that the difference between the linear source solution and the reference is more or less independent of the angular expansion order. Unlike the flat source, this indicates that the solution is well converged regardless of the angular expansion being used.

The computational efficiency examined in this work focuses on two important parameters: run time and memory requirements. In the case of the latter, the memory requirements for the linear source case are three times that of the flat source. Since the number of angular moments of the flux with respect to the anisotropic expansion order increases with expansion order, the linear source in this case will require three times the number of flux moments. Furthermore, in order to improve the computational efficiency, various quantities, such as the quantities defined by Eqs. (14) and (15), are dependent on the angular direction. Hence, unlike the case of the linear source with isotropic scattering, the linear source scheme for anisotropic scattering does require significantly more memory storage, relative to flat source anisotropic scattering.

The flat and linear source run times, relative to the reference case, are plotted in Figure 4 and 5. The relative run time is defined as follows

$$Rel.Time = \frac{t}{t_{ref}}$$

where t corresponds to the flat or linear source run time and t_{ref} to the reference case run time. The relative run time for the flat and linear source cases are 0.5 or lower for any given anisotropic scattering expansion order. Increasing the angular expansion order for the anisotropic source does result in an increase of the relative run time. This is due to the fact that the evaluation of the anisotropic source becomes increasingly 'expensive', in the sense that more time is spent evaluating the source in each given direction. Furthermore, the evaluation of the anisotropic source for the linear source has to be performed three times, instead of a single instance as for the flat source.

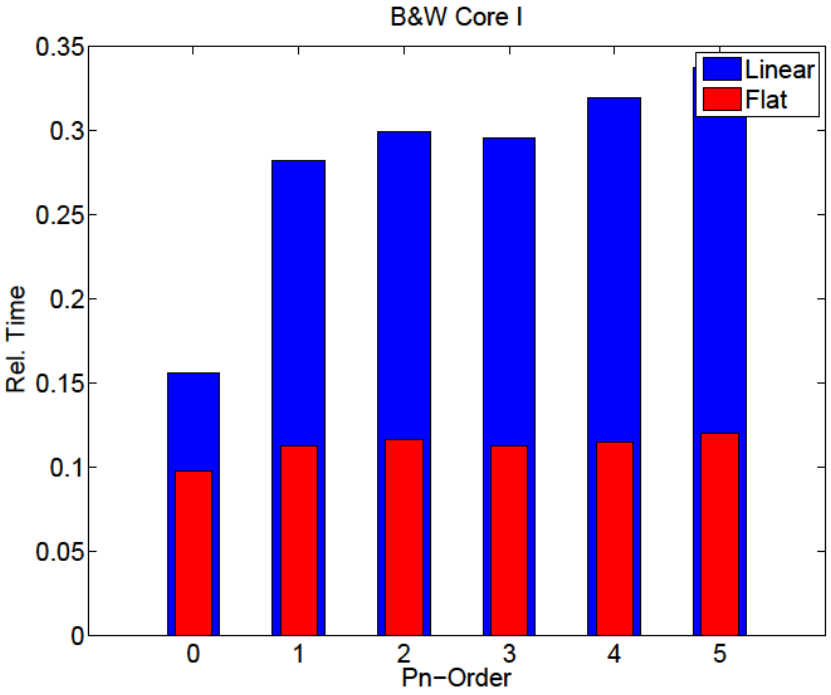

Figure 4. Core I flat and linear source relative (to reference) run time comparison.

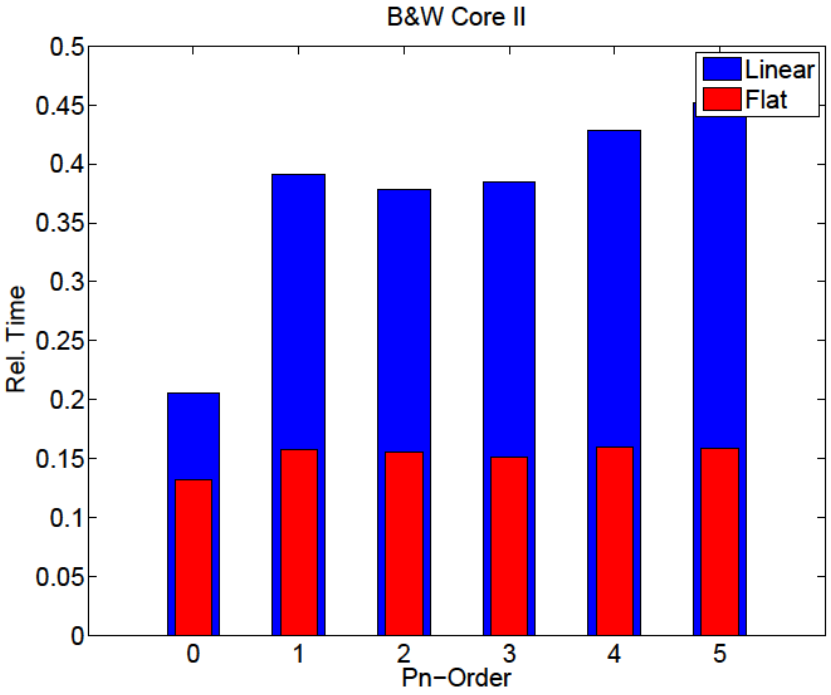

Figure 5. Core II flat and linear source relative (to reference) run time comparison.

5. CONCLUSIONS

Preliminary work has been completed in the development, implementation, and numerical testing of a spatially-linear source scheme that is compatible with anisotropic sources. The development of this scheme is an extension of the isotropic source case previous introduced in CASMO. This linear source scheme for anisotropic scattering is also fully compatible with CMFD acceleration. The use of the anisotropic source treatment in CASMO is relevant for benchmark purposes, especially in modeling critical assemblies. Numerical results present in this work indicate the advantage of the linear source for anisotropic scattering relative to the flat source treatment. In particular, results from the B&W simple criticals indicate that the linear source can reduce the error in the eigenvalue by as much as 288 pcm, relative to a fine-mesh flat source reference case. Furthermore, the linear source can reduce the run time by a factor of 3 relative to the fine-mesh reference case. Future work will address the reduction in memory requirements by assuming a spatially linear source for the low order angular flux moments while leaving the rest of the angular moments spatially flat, e.g. spatially linear source for angular moment l=0, and spatially flat for l=1 through L.

REFERENCES

[1] R. Ferrer, J. Rhodes, K. Smith, "Linear Source Approximation in CASMO5", Proc. Int. Conf. *PHYSOR 2012*, ANS, Knoxville, TN USA, April 15-20 (2012)

[2] R. Askew, "A Characteristic Formulation of the Neutron Transport Equation in Complicated Geometries", AEEW-M, 1108 (1972)

[3] M. J. Halsall, "CACTUS, A Characteristics Solution of the Neutron Transport Equation in Complicated Geometries", AEEW-R-1291, U.K. Atomic Energy Authority (1980)

[4] K. S. Smith, J.D. Rhodes, "Full-Core, 2-D, LWR Core Calculations with CASMO-4E", Proc. Int. Conf. *PHYSOR 2002*, Seoul, Korea, October 7-10 (2002)

[5] T. Bahadir, S-O Lindahl, "Studsvik's Next Generation Nodal Code SIMULATE5", Proc. Int. Conf. *2009 Advances in Fuel Management IV*, Hilton Head Island, SC USA, April 12-15 (2009)

[6] A. Yamamoto, Y. Kitamura, Y. Yamane, "Simplified Treatments of Anisotropic Scattering in LWR Core Calculations", *Journal of Nuclear Science and Technology*, **45:3**, pp. 217 – 229. URL http://dx.doi.org/10.1080/18811248.2008.9711430 (2008)

[7] J. Rhodes, K. Smith, and D. Lee, "CASMO-5 Development and Applications", Proc. Int. Conf. *PHYSOR-2006*, Vancouver, BC, Canada, September 10-14 (2006)

[8] P. Petkov, T. Takeda, "Transport Calculations of MOX and UO_2 Pin Cells by the Method of Characteristics", *Journal of Nuclear Science and Technology*, **35:12**, pp. 874-885, URL http://dx.doi.org/10.1080/18811248.1998.9733960 (1998)

[9] S. Santandrea, R. Sanchez, P. Mosca, "A Linear Surface Characteristics Scheme for Neutron Transport in Unstructured Meshes", *Nucl. Sci. Eng.*, **160**, pp. 22-40 (2008)

[10] E. Masiello, R. Clemente, S. Santandrea, "High-Order Method of Characteristics for 2-D Unstructured Meshes", Proc. Int. Conf. on *Mathematics, Computational Methods & Reactor Physics (M&C 2009)*, Saratoga Springs, NY USA May 3-7 (2009)

[11] M. N. Baldwin, M. E. Stern, "Physics Verification Program, Part III, Task 4, Summary Report", Babcock and Wilcox Report, BAW-3647-20 (1971)